

Factors Influencing Localized Corrosion of Mild Steel in Marginally Sour Environments

Wei Zhang, Bruce Brown, David Young, Srdjan Nestic, Marc Singer
Institute for Corrosion and Multiphase Technology, Ohio University,
342 West State Street, Athens, OH, 45701, USA

ABSTRACT

A comprehensive parametric study was performed using a small-scale laboratory setup with the aim of investigating the occurrence of localized corrosion in marginally sour environments. The parameters of interest were the partial pressure of H₂S, bulk pH, temperature, the partial pressure of CO₂, salt concentration and steel substrate carbon content. This series of experiments defined a window of operating conditions leading to the occurrence of localized corrosion: temperatures between 30°C and 60°C, p_{H₂S} from 0.02 mbar to 0.15 mbar, bulk pH below 6, and sodium chloride concentrations between 1 and 10 wt%. Even if, according to thermodynamic calculations, FeS_{Mackinawite} was under-saturated in the bulk solution in marginally sour environments, the formation of an FeS_{Mackinawite} layer was observed by scanning electron microscope (SEM) and Element Energy Dispersive Spectroscopy (EDS), embedded in the Fe₃C network of the steel microstructure. The hypothesis is that the surface saturation of FeS_{Mackinawite} was much higher than in the bulk due to mass transfer limitations within the Fe₃C network leading to a higher pH. This hypothesis was confirmed when similar experiments did not yield any localized corrosion when performed on 99% pure iron samples, whose microstructure does not contain any cementite.

Keywords: Localized Corrosion, Pitting, Sour Corrosion, FeS, H₂S, CO₂ corrosion, Fe₃C, Mild Steel, API X65 Steel, Pure Iron.

INTRODUCTION

Localized corrosion is a common failure mode in sour environments¹ found in oil and gas pipelines containing CO₂, H₂S, and brine. For instance, the Caroline oil spill at Sundre, Alberta, Canada on Jan 6, 1994, was caused by internal wet H₂S and CO₂ pitting corrosion at the bottom of the pipeline, where an extremely high pitting corrosion rate, approximately 30 mm/y, was observed.² Researchers in the Institute for Corrosion and Multiphase Technology (ICMT) at Ohio University have reproduced localized corrosion in CO₂ environments with low concentrations of H₂S^{3,4,5,6,7} commonly found in the oil and gas industry. Although these studies identified certain sets of experimental conditions that seem to lead to the occurrence of localized corrosion, the window of operating conditions leading to the occurrence of localized corrosion is not properly defined yet.

When investigating localized/pitting corrosion of steel, it is tempting to refer to the well-established theory of localized corrosion of stainless steel in an atmospheric environment (iron-oxygen-brine

system), involving the disruption of the passive layer and pit acidification.^{8,9} Passive layers are complicated multilayer structures on a nanometer scale¹⁰, composed of oxides and hydroxides. However, these mechanisms cannot be applied to localized corrosion of mild steel in sour environments containing both H₂S and CO₂ forming a buffered environment, where there are no ferric species and pit acidification is not possible. Furthermore, the much thicker corrosion product layers that form on mild steel (sulfides and carbonates) do not qualify as passive films although they can be protective in some cases. Corrosion products in sour environments are thought to contain at least one polymorph of FeS, such as mackinawite, pyrite, pyrrhotite, or greigite, depending on environmental conditions such as temperature and exposure time, although there are still different mechanisms proposed.¹¹ Research on structure and morphology of the corrosion product layers related to localized corrosion in marginally sour environments is scarce. Therefore, any mechanistic study of the phenomenon should begin with a systematic evaluation of the controlling factors.

Localized corrosion mechanism is typically described as a three-step phenomenon: protective layer formation; pit initiation (generation); pit propagation or annihilation.

Layers formed on the surface of mild steel in marginally sour environments might contain several types of corrosion products:

FeCO₃: Most crude oil and natural gas contain CO₂. Consequently, in aqueous environments, iron carbonate (siderite) is commonly found as a corrosion product on the steel surface.

FeS: Some systems additionally contain H₂S, which can form an iron sulfide (Fe_xS_y) corrosion product layer. Iron sulfide refers to a range of chemical compounds composed of iron and sulfur. In the sour corrosion of steel, mackinawite is the fastest forming corrosion iron sulfide. A comparison between the iron carbonate and mackinawite corrosion products' formation mechanism is shown in Table 1. It will be elaborated on in the following paragraphs.

Fe₃C: Iron carbide (cementite) is a component of the steel microstructure. It does not readily corrode and remains as a residue on the steel surface after the ferrite (α -Fe) phase is dissolved. Corrosion products such as iron carbonate and iron sulfide can precipitate within the exposed Fe₃C network, thus making it an important constituent of the protective surface layers in sour corrosion.

Fe₃O₄: According to thermodynamic calculations, magnetite (Fe₃O₄) can be formed in sweet as well as sour environments at high temperature. For example, Han reported that magnetite was detected in an iron carbonate corrosion product layer formed on steel exposed to a CO₂ containing aqueous solution at T=80°C, pH ranges from 7.1~8.1, pCO₂ 0.53 bar, NaCl 1 wt.%, in stagnant conditions.¹²

Knowledge on FeCO₃ layer and FeS layer growth mechanisms has been accumulated after several decades of systematic research on CO₂ and H₂S corrosion. The key points are summarized in Table 1. For FeCO₃, it is agreed that the layer is formed by precipitation¹³, as shown in Equation (1). The driving force of precipitation is the degree of saturation of FeCO₃ in aqueous solution.¹⁴ FeCO₃ precipitates when saturation degree is greater than unity as shown in Equation (2). The layer growth rate is related to the activation energy and the aforementioned degree of saturation, as shown in Equation (3). This corrosion product layer can be “undermined” by corrosion of the underlying steel if the ratio of precipitation to corrosion rates is near or less than unity, as referenced by Equation (4). This “undermining effect” was proposed as an initiation mechanism for localized corrosion in sweet (CO₂ only, no H₂S) environments¹⁴.

As for FeS, it is thought that Mackinawite (written as FeS_{mackinawite}) always forms first, and then is converted into other forms of iron sulfide. Sun¹⁵ proposed a mechanisms of iron sulfide layer formation at the steel surface, by direct reaction between H₂S and the iron in the steel forming a thin layer that spalls and reforms, to produce a thicker outer layer of iron sulfide. Zheng further developed the “two layers” theory and proposed that inner layer forms by chemisorption^{16,17} (Equation 9) while the outer layer forms by precipitation¹⁸ (Equation 5). This chemisorbed layer is also considered to be very thin; on the order of nanometers and directly interferes with the charge transfer reactions at the steel interface. The outer precipitated layer of FeS that is found on top of the chemisorbed layer is driven by the saturation degree of Fe²⁺ and S²⁻ in aqueous solution near the steel surface (Equation 5).¹⁸ The

precipitated layer thickness is usually measured on a micron scale, and its growth rate can be defined by a precipitation rate^{18,19} (Equation 7).

Localized corrosion is usually thought to happen due to a localized failure of a protective surface layer of some kind. In the case of steel corroding in H₂S containing aqueous solutions, it remains unknown which of the two layers plays a more important role in localized corrosion. The characteristics of the protective layers are thought to govern whether or not localized corrosion will occur and to determine what mechanisms are involved. Therefore, layer growth mechanisms, kinetics, morphology, and phase identity constitute a major focus of this localized corrosion study. There are two main effects introduced by the growth of corrosion products layers.¹⁸ The first effect is the direct influence of the chemisorbed layer on the charge transfer reactions. The second effect is the impediment of mass transfer by the outer porous iron sulfide layer, which determines the species concentration near the steel surface which can be very different from that in the bulk solution. The extent of the difference between the bulk and surface conditions depends on porosity (ϵ), tortuosity (τ) and thickness (δ_s) of the corrosion product layer. Therefore, these characteristics of the layer will affect both the layer growth kinetics and the corrosion rate. Conversely, understanding the mechanisms of corrosion, corrosion product layer formation, and surface water chemistry are essential to understanding the localized corrosion mechanisms in sour environments.

Table 1
FeCO₃ Layer and FeS Layer Growth Mechanism¹⁸

| | in CO ₂ Corrosion (by precipitation) | in H ₂ S Corrosion (by precipitation) | in H ₂ S Corrosion (by chemisorption) |
|-------------------------------|--|---|--|
| Layer Formation | <u>Equation 1:</u> $\text{Fe}_{(\text{aq})}^{2+} + \text{CO}_{3(\text{aq})}^{2-} \rightleftharpoons \text{FeCO}_{3(\text{s})}$ | <u>Equation 5:</u> $\text{Fe}_{(\text{aq})}^{2+} + \text{S}_{(\text{aq})}^{2-} \xrightleftharpoons{K_{\text{sp},\text{s}^{2-}}} \text{FeS}_{(\text{s})}$ | <u>Equation 9:</u> $\text{Fe}_{(\text{s})} + \text{H}_2\text{S}_{(\text{aq})} \rightarrow \text{FeS}_{(\text{ad})} + 2\text{H}_{(\text{ad})}$ |
| When does the layer form? | <u>Equation 2:</u> $S_{\text{FeCO}_3} = \frac{[\text{Fe}^{2+}][\text{CO}_3^{2-}]}{K_{\text{sp, FeCO}_3}} > 1$ | <u>Equation 6:</u> $S_{\text{FeS}} = \frac{[\text{Fe}^{2+}][\text{HS}^-]}{K_{\text{sp, FeS}(\text{HS}^-)}} > 1$ | When H ₂ S chemisorbs on the steel surface |
| How fast does the layer form? | <u>Equation 3:</u> $\text{PR}_{\text{FeCO}_3(\text{s})} = e^{28.2 - \frac{54851.4}{\text{RT}}} \frac{\text{S}}{\text{V}} K_{\text{sp, FeCO}_3} (S_{\text{FeCO}_3} - 1)$ | <u>Equation 7:</u> $\text{PR}_{\text{FeS}(\text{s})} = e^{48 - \frac{40000}{\text{RT}}} \frac{\text{S}}{\text{V}} K_{\text{sp, FeS}} (S_{\text{FeS}} - 1)$ | Very fast |
| Is this layer protective? | <u>Equation 4:</u> $\text{Scaling Tendency} = \frac{\text{Precipitation Rate}}{\text{Corrosion Rate}}$ | <u>Equation 8:</u> $\text{Scaling Tendency} = \frac{\text{Precipitation Rate}}{\text{Corrosion Rate}}$ | Yes - decreases the rate of electrochemical reactions |

A number of parameters/phenomena should be investigated to develop a mechanistic understanding of the initiation and propagation of localized corrosion of mild steel in marginally sour environments:

- local conditions at the steel surface,
- characteristics of the formed layers (composition, structure, protectiveness), and whether they are the product of precipitation or chemisorption,
- processes related to the formation of defects in the layer, eventually leading to pit initiation,
- criterion for pit propagation/annihilation.

In this paper, a comprehensive parametric study was performed using a small-scale laboratory setup with the aim of investigating the occurrence of localized corrosion in marginally sour environments. The parameters of interest were partial pressure of H₂S, bulk pH, temperature, partial pressure of CO₂, salt concentration and the different type of materials and carbon content/microstructure of the metal. This series of experiments defined a window of operating

conditions leading to the occurrence of localized corrosion, characterized the corrosion product layer structure, and identified mechanisms related to the initiation and propagation of localized corrosion.

EXPERIMENTAL PROCEDURE

Experiments were conducted at atmospheric pressure in a 2-liter glass cell (Figure 1) with a 1wt% NaCl in deionized water solution. Gas (a mixture of hydrogen sulfide, H₂S and carbon dioxide, CO₂) was sparged through the cell continuously. A three-electrode setup was used. A static cylindrical electrode was used as the working electrode (WE). A platinum wire was used as a counter electrode (CE). A saturated silver-silver chloride (Ag/AgCl) reference electrode (RE) was connected to the cell externally via salt bridge with a Luggin capillary. A 2-inch magnetic stir bar at the bottom of the glass cell was used for mixing the solution. The concentration of H₂S was adjusted with the help of a gas rotameter and measured when exiting the cell by a gas sampling pump with H₂S colorimetric detector tubes. A carbon scrubber was used to treat the gas coming out of glass cell to remove the H₂S. Automatic control of pH was achieved by pumping the solution through an ion exchange resin column.

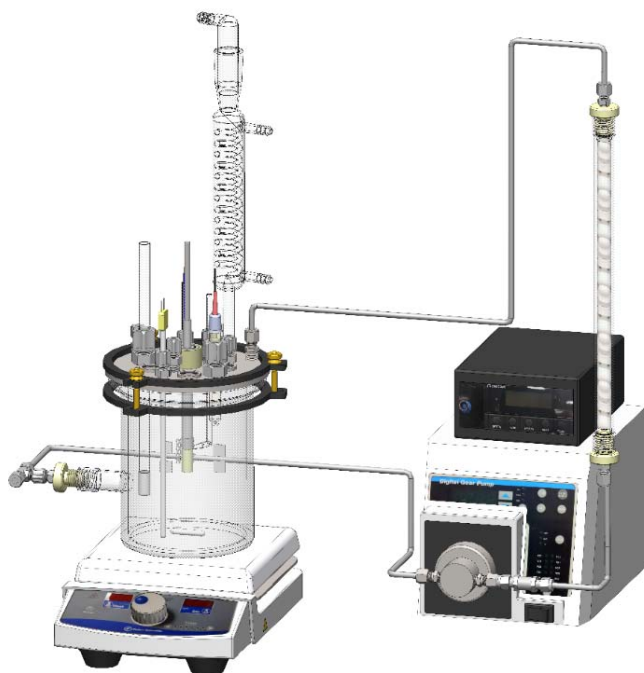


Figure 1. Experimental setup for the two-liter glass cell using a stable solution chemistry system for small-scale tests.²⁰ (Image courtesy of Cody Shafer, ICMT)

Experimental Matrix

The test matrix (Table 2) was designed to develop an experimental database to study mechanisms of localized corrosion in marginally sour environments. The following parameters were investigated: pH₂S, pCO₂, pH, temperature, salt concentration, and different types of materials (carbon content/microstructure) of the metal substrate .

Table 2
Effect of pH, Temperature, Salt Concentration, and Different Types of Materials (carbon content/microstructure).

| | Baseline | pH ₂ S | | | | pCO ₂ | | | Solution pH | | Temperature | | NaCl wt.% | | Material | Exposure Time |
|----------------------------|----------|-------------------|-------------|-------------|-------------|------------------|-------------|-------------|-------------|-----------|-------------|------|-----------|-----------|------------------|---------------|
| | | | | | | | | | | | | | | | | |
| Temperature/°C | 30 | 30 | | | | 30 | | | 30 | 60 | 80 | 30 | | 30 | 30 | |
| pH | 5 | 5 | | | | 5 | | | 4 | 6 | 5 | | 5 | 5 | 5 | |
| pCO ₂ /bar | 0.96 | 0.96 | | | | 0 | 0.53 | 0.82 | 0.96 | | 0.8 | 0.53 | 0.96 | | 0.96 | 0.96 |
| pH ₂ S/mbar | 0.04 | 0 | 0.02 | 0.09 | 0.15 | 0.04 | | | 0.04 | | 0.03 | 0.02 | 0.04 | | 0.04 | 0.04 |
| pH ₂ S/ppm | 40 | 0 | 20 | 90 | 150 | 40 | | | 40 | | 40 | | 40 | | 40 | 40 |
| WE Material | X65 | X65 | | | | X65 | | | X65 | | X65 | | X65 | | Pure Iron | X65 |
| NaCl Concentration/ (wt.%) | 1 | 1 | | | | 1 | | | 1 | | 1 | | 0 | 10 | 1 | 1 |
| Exposure Time/day | 7 | 7 | | | | 7 | | | 7 | | 7 | | 7 | | 7 | 14 |

Material

The composition of the API 5L X-65²¹ steel used in the present experiments is shown in Table 3. It has a ferrite pearlite microstructure as shown in Figure 2. The working electrode was machined from the parent steel material and had a diameter of 1.20 cm and a working surface area of 5.4 cm².

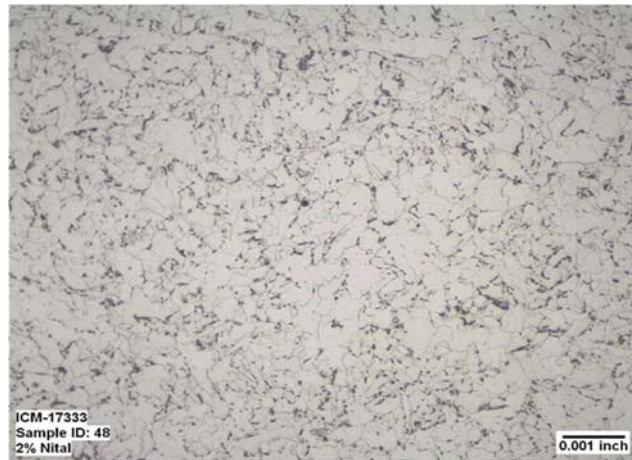


Figure 2. Microstructure of X65 (0.05 wt. % C) consists of ferrite pearlite²²

Table 3
Chemical Composition (wt. %) of X65.

| | | | | | | | | | |
|-------|--------|-------|-------|-------|-------|------|-------|---------|-------|
| Al | As | C | Co | Cr | Cu | Mn | Mo | Nb | Ni |
| 0.033 | 0.015 | 0.05 | 0.012 | 0.150 | 0.140 | 1.51 | 0.160 | 0.03 | 0.380 |
| P | S | Sb | Si | Sn | Ti | V | Zn | Fe | |
| 0.004 | <0.001 | 0.035 | 0.250 | 0.012 | 0.01 | 0.04 | 0.004 | balance | |

Procedure

The aqueous solution was initially purged with CO₂ gas for at least three hours to remove oxygen. After the solution was deoxygenated, H₂S was added by purging for at least half an hour to saturate the solution at the required partial pressure of H₂S. H₂S gas concentration was adjusted by purging different ratios CO₂ and H₂S, from 100 ppm_(v) to 10 vol.% H₂S, corresponding to a H₂S partial pressure p_{H₂S} = 0.1 mbar and 96.5 mbar respectively, at 30°C. The pH was adjusted by adding deoxygenated hydrochloric acid or sodium hydroxide. Prior to immersion, the mild steel specimen surfaces were polished with 400 and 600 grit sandpaper, rinsed with alcohol and dried with an air blower.

Polarization resistance (Rp) measurements were conducted by polarizing the WE ± 5 mV from the open circuit potential and scanning at 0.125 mV/s. Solution resistance was measured independently using electrochemical impedance spectroscopy (EIS), and the measured Rp was then corrected. The linear polarization resistance (LPR) constant B = 23 mV/decade used in this work was determined from longer-term weight loss measurements. EIS measurements were carried out by applying an oscillating potential ± 5 mV around the open circuit potential of the WE, using the frequency range 0.01Hz to 5kHz.

Multiple measurements were made for each experiment. General corrosion rate was measured by LPR and weight loss method. Pit penetration rate and pitting density were measured by a high resolution optical profilometer after the corrosion product layer on the specimen was removed by Clarke solution treatment.²³ SEM and EDS were used to study the corrosion product layer structure and composition. Ferrous ion concentration was measured by Spectrophotometer and 1,10 phenanthroline method using a multipoint standard adsorption curve at 510nm. A 10 ml solution sample from the test was used along with deionized water as the control for the spectrophotometer. Multiple measurements were used for repeatability of results.

Considering the somewhat subjective nature of the definition of localized corrosion,²² a rule has been developed to help decide whether localized corrosion occurred or not. As demonstrated in Figure 3 (left), after exposure to the corrosive environment, samples suffer from both general metal loss and localized attack. General metal loss can be calculated from total mass loss (Equation 10); while localized attack must be evaluated by profilometry to quantify the maximum depth (Equation 11); then the ratio of pit penetration rate divided by general corrosion rate is the judging criteria (Table 4). According to Table 4, when this ratio is:

- smaller than 3, the corrosion is judged to be uniform;
- larger than 5, localized corrosion occurs;
- between 3~5, localized corrosion initiated but may not be sustained.

Last, but not least, this criterion only applies to pits that are deeper than 10 μm in order to distinguish them from general surface roughening. Figure 3 (right) demonstrates the optical profilometry measurements that can identify the maximum pit depth. The measured three-dimensional image of localized corrosion is illustrated by a color scale with the measured depth shown in the line profile below.

$$\text{Weight Loss Corrosion Rate} \left(\frac{\text{mm}}{\text{y}} \right) = \frac{\text{Measured Weight Loss}}{\text{Time}} \quad (10)$$

$$\text{Penetration Rate} \left(\frac{\text{mm}}{\text{y}} \right) = \frac{\text{Measured Pit Depth}}{\text{Time}} \quad (11)$$

$$\text{Pitting Ratio} = \frac{\text{Penetration Rate}/(\text{mm}/\text{y})}{\text{Weight Loss Corrosion Rate}/(\text{mm}/\text{y})} \quad (12)$$

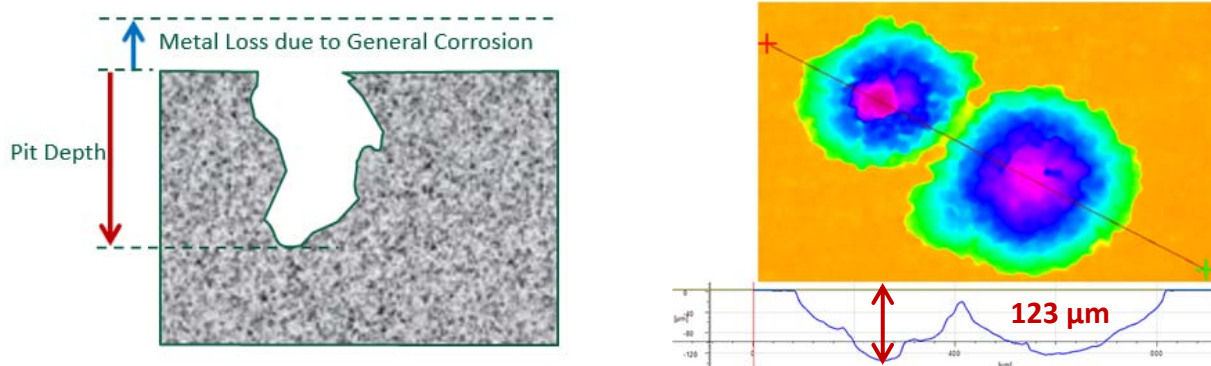


Figure 3. Pit depth and General Corrosion

Table 4

Judging Criteria for Localized Corrosion*

| | |
|-----------------------|------------------------------|
| Pitting Ratio < 3 | No localized corrosion |
| 3 < Pitting Ratio < 5 | Possible localized corrosion |
| Pitting Ratio > 5 | Localized corrosion |

*Applies only to measured pit depth >10 μm

RESULTS

Effect of H₂S Partial Pressure on Localized Corrosion

Experimental results obtained with 0, 20, 40, 90, & 150 ppm of H₂S were compared to identify the lower and upper limits of pH₂S under which localized corrosion occurs at 30°C, ~1 bar CO₂. Figure 4 shows bulk saturation degree for both mackinawite, S(FeS_{mackinawite}), and iron carbonate, S(FeCO₃). During each experiment at a specific H₂S partial pressure, the measured bulk ferrous ion concentration increased from zero at the beginning of the test, and then reached a stable value, usually after 4 days of exposure, as indicated by the vertical lines in Figure 4. Figure 4 also shows a comparison of these values to the saturation line where FeS_{mackinawite}=1. This blue line shows at each H₂S partial pressure, how much [Fe²⁺] is needed to reach saturation. The orange line is the calculated saturation limit where S(FeCO₃) = 1. The S(FeCO₃) line is depicted as a horizontal line here since pCO₂ was the same for this series of experiments. In all the five experiments, the bulk ferrous ion concentration was less than the concentration necessary to reach the saturation value of 1 for either S(FeS_{mackinawite}) or S(FeCO₃). Therefore, no precipitated layer was expected in any of these experiments based on bulk water chemistry conditions.

SEM images in Figure 5 reveal first that a relatively thick layer was formed in the absence of H₂S while no layer or a very thin layer was found for the other cases with H₂S. More importantly, it indicates that extensive localized corrosion occurred with 20 and 40 ppm H₂S but not in the other conditions, consistent with the findings of Navabzadeh Esmaeely⁵. In addition, the cross-section images also show the morphology of those pits which seems to be mainly semi-hemispherical and filled with FeS deposited on the Fe₃C network. A thin layer of corrosion product (most likely FeS) was left at the top of the pit. However, the resolution of these SEM images is not high enough to determine whether the thin layer exists on the remaining steel surface not affected by localized corrosion.

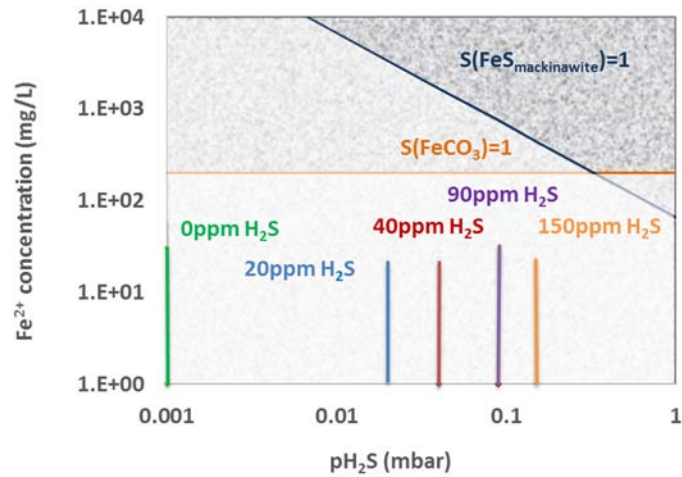


Figure 4. Saturation degree of the bulk solution of both mackinawite (blue line and above) and FeCO_3 (orange line and above) of different pH_2S . (X65 carbon steel, 30°C , $\text{pH}5$, 0.97 bar CO_2 , 0 to 0.15 mbar H_2S , $1\text{wt.}\%$ NaCl , 300rpm stir bar, 7 days exposure.)

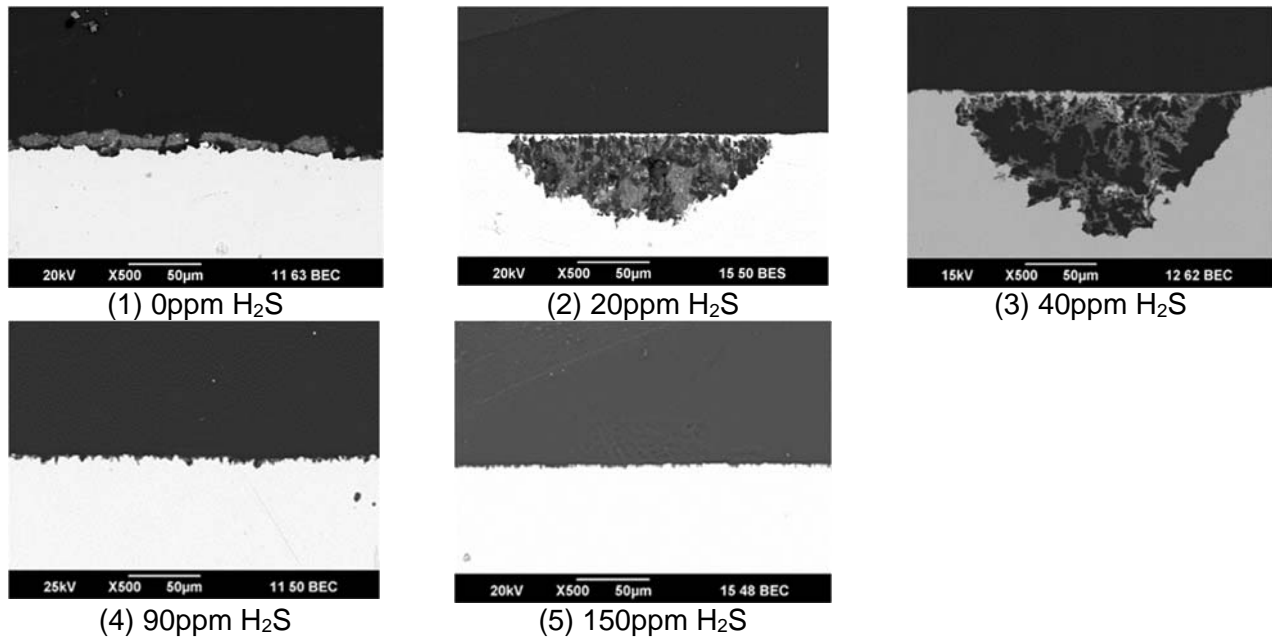


Figure 5. SEM cross-section images of specimens at different H_2S partial pressure after 7 days exposure. (X65 carbon steel, 30°C , $\text{pH}5$, 0.97 bar CO_2 , 0 to 0.15 mbar H_2S , $1\text{wt.}\%$ NaCl , 300rpm stir bar, 7 days exposure.)

Surface profilometry images of the corroded specimens after corrosion product layer removal by Clarke solution treatment are displayed in Figure 6. Extremely High pitting density was observed at 20 ppm and 40ppm H_2S . Lower pitting density was observed at 90 ppm H_2S . No localized corrosion was found within the entire specimen surface at 0 and 150 ppm H_2S .

The error margins listed in caption of Figure 6 was calculated is as follows. Each experiment was repeated, so the reported (general) corrosion rate is the average value for the two specimens. The error margin denotes the minimum and maximum experimental measurements. The pit penetration rates were based on the deepest pit found only on one of the two specimens. The margin of error is calculated based on the vertical resolution of the measurements.

The general corrosion rates were determined by weight loss. The CO₂ only (0ppm H₂S) experiment yielded the highest general corrosion rate, 2~2.5 mm/y. Adding 20ppm of H₂S led to a considerable reduction in the general corrosion rate to less than 1.0 mm/y, although in some cases severe localized corrosion slightly affected the calculations. In general, the higher the H₂S content in the gas phase was, the lower the general corrosion rates became.

According to the criteria defined in Table 4, the specimens exposed to 20, 40 and 90ppm H₂S clearly experienced localized corrosion although the pitting density for the 90ppm H₂S was very low.

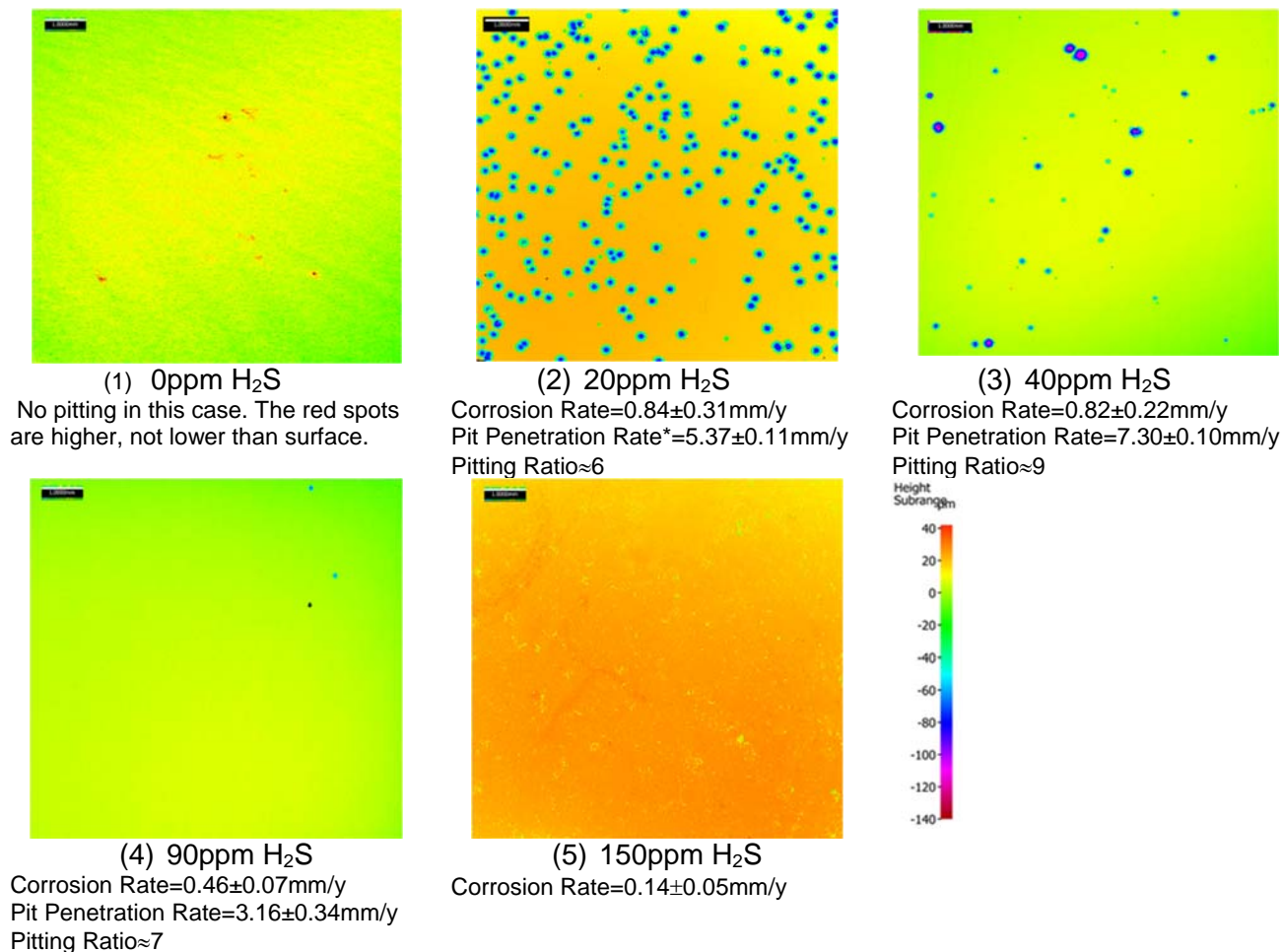


Figure 6. Surface profilometry analysis of specimens recovered for each test condition after 7 days exposure after corrosion product layer removed. (X65 carbon steel, 30°C, pH5, 0.97 bar CO₂, 0, 0.02, 0.04, 0.09, & 0.15 mbar H₂S, 1 wt.% NaCl, 300rpm stir bar)

Localized corrosion can be related to the presence of a corrosion product layer on the steel surface but none were observed on the specimens for the 20, 40, and 90 ppm H₂S experiments. In addition, Figure 4 suggests that FeS should not be saturated in the bulk solution which further may suggest that there should be no precipitated corrosion product layer. However, corrosion could lead to a much higher FeS saturation level at the surface and facilitate a limited FeS precipitation. Whether the occurrence of localized corrosion is due to failure of the chemisorbed layer or of a very thin precipitated layer is not clear at this stage.

Effect of pCO₂ on Localized Corrosion

The effect of pCO₂ on the localized corrosion in sour environments was determined by running a series of tests under 0 to 0.97 bar of CO₂ and at a fixed H₂S content 0.04 mbar (40 ppm). Figure 7 shows the saturation degree for both mackinawite and iron carbonate. This time, the partial pressure of H₂S is

shown as a straight horizontal line since it was set to a fixed value while the partial pressure of CO₂ was varied. In all of these experiments, the measured bulk ferrous ion concentration was again always lower than the concentration required to reach the saturation value of 1 for either S(FeS_{mackinawite}) or S(FeCO₃). Consequently, no precipitation was expected for these experiments based on bulk water chemistry conditions.

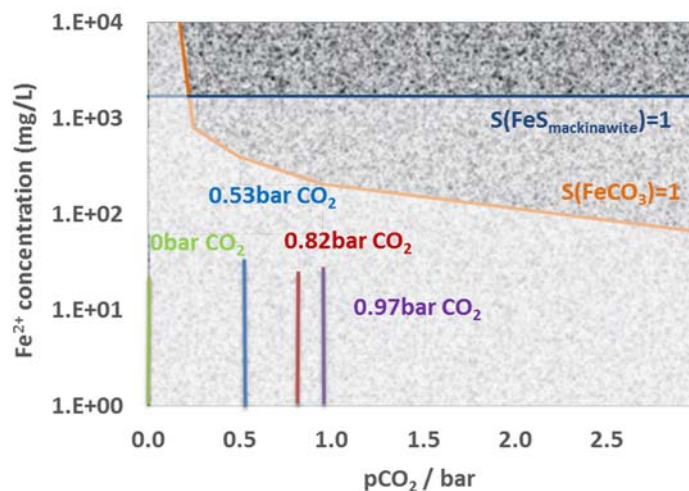


Figure 7 . Saturation degree of bulk solution for both mackinawite, $S(\text{FeS}_{\text{mackinawite}})$, [blue line and above] and iron carbonate, $S(\text{FeCO}_3)$, [orange line and above] for varied $p\text{CO}_2$. (X65 carbon steel, 30°C, pH5, 0/0.53/0.82/0.97 bar CO₂, 0.04mbar H₂S, 1 wt.% NaCl, 300rpm stir bar)

Profilometry images (Figure 8) show occurrence of localized corrosion in all the cases that contained CO₂. In a H₂S only environment where the $p\text{CO}_2=0$ bar (Figure 9(1)), very small indications of pit initiation (10~20 μm deep) were observed, but were too small to be considered as true localized corrosion. Fang, et al., also had similar findings in an H₂S only corrosion study²⁴. This suggests that localized corrosion may initiate from the presence of H₂S, but does not propagate without the presence of CO₂. A similar pitting density, independent of $p\text{CO}_2$, was observed for the different conditions. This finding supports the hypothesis that localized corrosion in sour environments is influenced by the FeS_{mackinawite} layer rather than the iron carbonate layer. However, propagation of the localized corrosion seems to be independent from the CO₂ content, in this narrow range of conditions. This is demonstrated by the fact that pit penetration rates in the 0.53 bar and 0.82 bar $p\text{CO}_2$ experiments were smaller than in the 0.97 bar $p\text{CO}_2$ experiment. Overall, the occurrence of localized corrosion indicated that a corrosion product layer formed even though the bulk solution $S(\text{FeCO}_3) < 1$ and $S(\text{FeS}_{\text{mackinawite}}) < 1$. Defects in this layer led to localized corrosion initiation. The possible explanation is that the surface saturation degree of FeS_{mackinawite} was actually greater than bulk FeS saturation and led to formation of a partially protective corrosion product layer.

Figure 9 shows SEM cross-section images of specimens collected at different $p\text{CO}_2$ for experiments (0.04 mbar pH₂S, 30°C, and 7 days exposure). For the specimens obtained with 0.53 bar and 0.97 bar $p\text{CO}_2$, large pits were easily captured in the cross-sectional analysis. No pit was captured on the polished cross section of the 0.82 bar CO₂ specimen, although there should have been some according to the surface profilometry results in Figure 8. Again, localized corrosion initiation (10~15 μm deep pit) was observed for the test at $p\text{CO}_2=0$ bar. Specimens were pulled out after one, three and seven days' exposure, however, the pit depths found on these samples were almost the same, and within the surface roughness fluctuation. Therefore, at $p\text{CO}_2=0$ bar localized initiation may have happened but without further propagation.

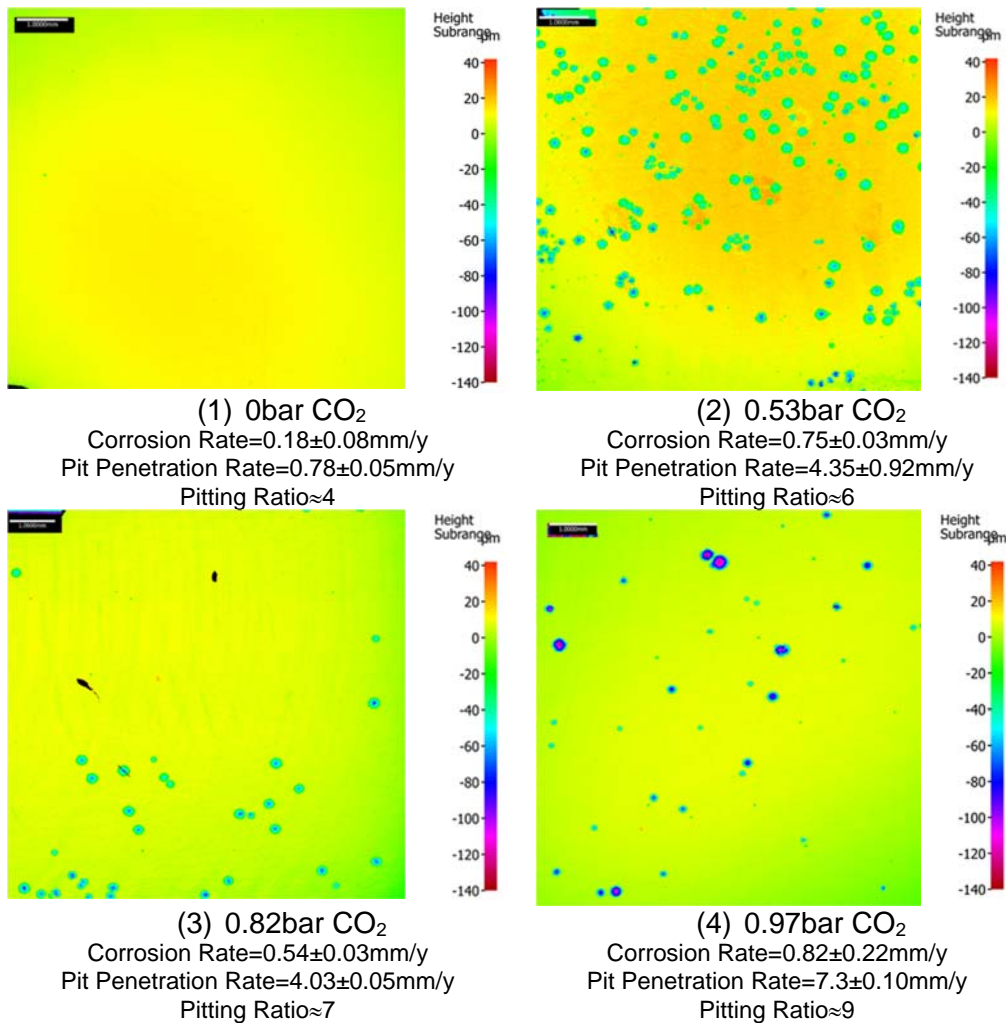


Figure 8. Surface profilometry analysis of specimens recovered for each test condition after 7 days exposure after corrosion product layer removed. (X65 carbon steel, 30°C, pH5, 0/0.53/0.82/0.97 bar CO₂, 0.04mbar H₂S, 1 wt.% NaCl, 300rpm stir bar)

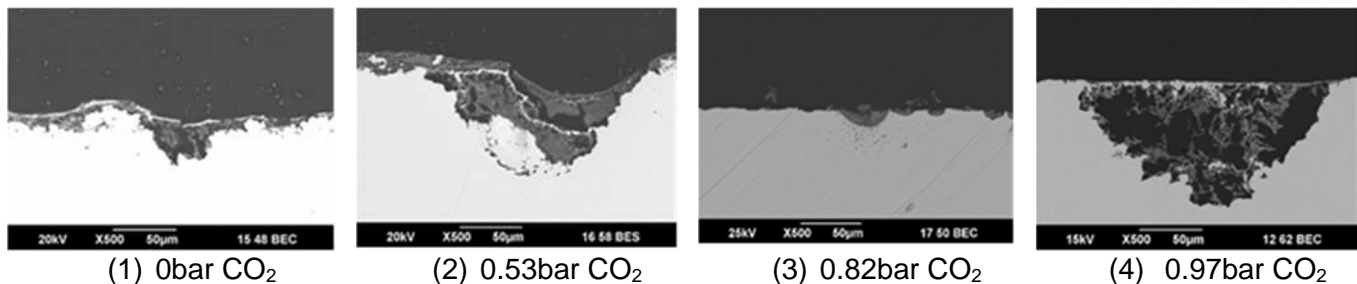


Figure 9. SEM cross-section images of specimens at different CO₂ partial pressure after 7 days exposure. (X65 carbon steel, 30°C, pH5, 0/0.53/0.82/0.97 bar CO₂, 0.04mbar H₂S, 1wt.% NaCl, 300rpm, 7days.)

Effect of pH on Localized Corrosion

The effect of pH on localized corrosion in sour environments was evaluated at bulk pH 4, 5 and 6. The vertical lines shown in Figure 10 represent the range of concentration of ferrous ions observed during each experiment. The saturation values for both mackinawite and iron carbonate are dependent upon solution pH. Lesser amount of ferrous ions was required to reach saturation at higher pH 6. Figure 10 shows that neither mackinawite nor iron carbonate achieved saturation in the experiments at pH 4 and

pH 5. At pH 6, $S(\text{FeCO}_3)$ in bulk solution exceeded the saturation value of 1, while $S(\text{FeS}_{\text{mackinawite}})$ was very close to saturation in the bulk solution during the experiment. This indicates that both corrosion products were most likely supersaturated at the steel surface. A protective layer made of FeS, possibly Fe_3C and FeCO_3 , was expected in the pH6 case. This protective layer may be the reason why no pitting was observed at pH 6, as shown in Figure 11 and Figure 12. The ferrous concentration never exceeds 30 ppm in all the experiments. Tiny black particles were observed in the bulk solution, which increased in amount with exposure time.

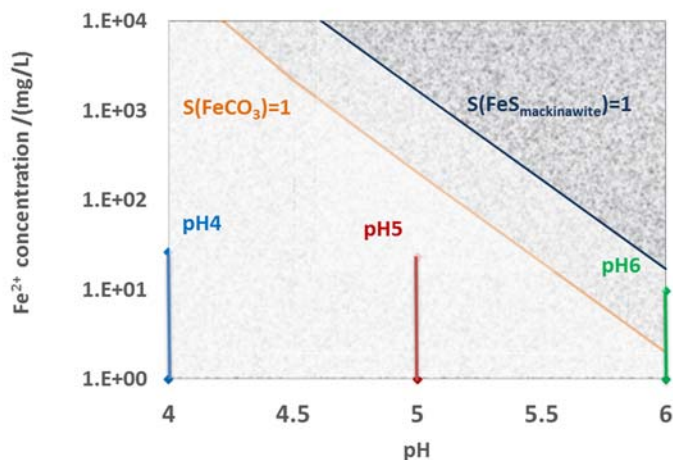


Figure 10. Saturation degree of both mackinawite (blue line and above) and FeCO_3 (orange line and above) in bulk solution. (X65 carbon steel, 30°C, pH4/5/6, 0.97 bar CO_2 , 0.04mbar H_2S , 1 wt.% NaCl, 300rpm, 7days.)

Figure 11 shows surface profilometry scanning results at different pHs after 7 days exposure and after removal of the corrosion product layer. Both severe general corrosion and pitting were observed on the pH4 specimen, while very low corrosion rate with no pitting was observed for the pH6 specimen.

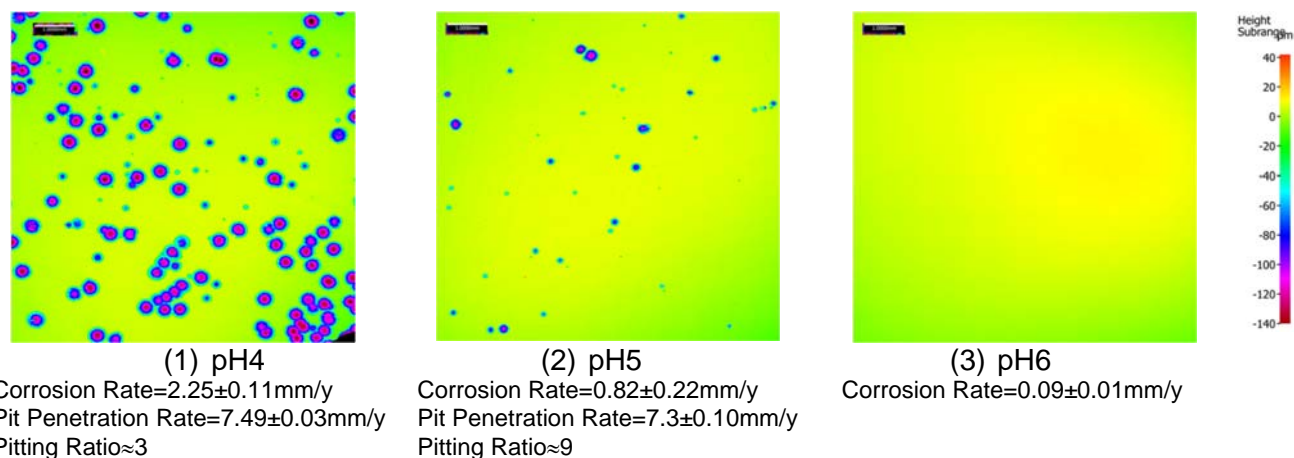


Figure 11. Surface profilometry analysis at different pH after 7 days exposure after corrosion product layer was removed. (pH=4/5/6, X-65 carbon steel, 30°C, 0.97 bar CO_2 , 0.04 mbar (40ppm) H_2S , 1 wt.% NaCl, 300rpm stir bar.)

Cross-section images in Figure 12 indicate that as the pH increased, the extent of localized corrosion and the uniform corrosion decreased. The scaling tendency also increased with increasing pH, which would indicate a more protective FeS layer at higher pH with no pit formation.

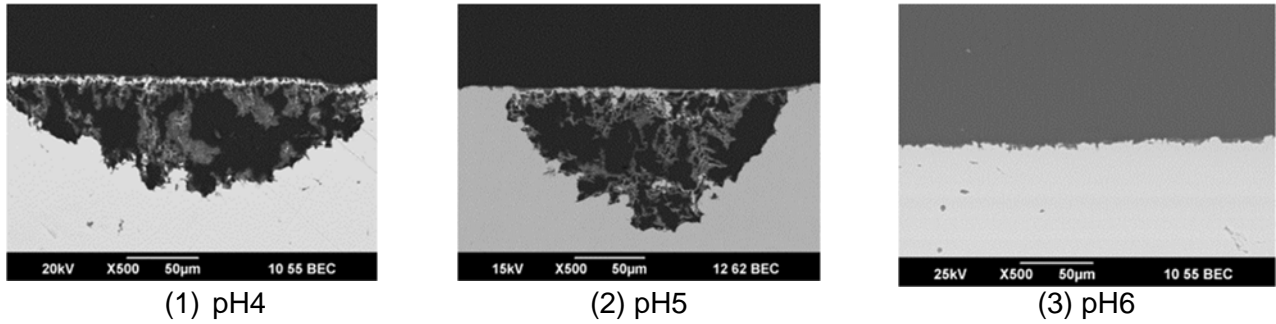


Figure 12. SEM cross-section images at different pH after 7 days exposure. (pH=4/5/6, X-65 carbon steel, 30°C, 0.97 bar CO₂, 0.04 mbar (40ppm) H₂S, 1 wt.% NaCl, 300rpm stir bar.)

Effect of Temperature on Localized Corrosion

The effect of temperature on the localized corrosion was investigated at 0.04 mbar (40 ppm) and H₂S and 0.53 bar of CO₂ by performing experiments at 30°C, 60°C, and 80°C. According to the water chemistry calculation for the bulk in Figure 13, the solution was under-saturated with respect to mackinawite and iron carbonate in experiments at 30°C, saturated only with respect to mackinawite at 60°C, and saturated with respect to both mackinawite and iron carbonate at 80°C.

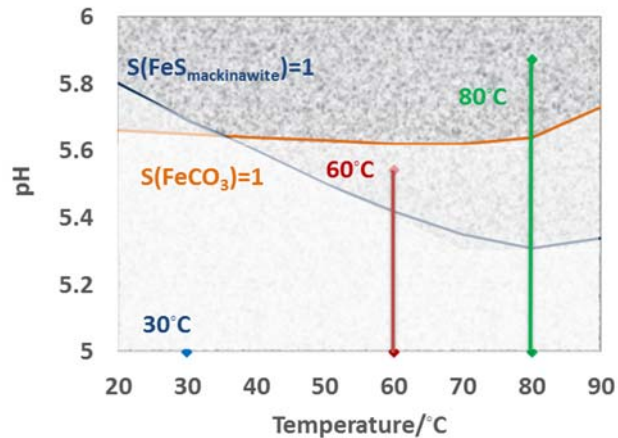


Figure 13. Saturation degree of both mackinawite (blue line and above) and FeCO₃ (orange line and above) in bulk solution. (X65 carbon steel, 30/60/80°C, target pH5, 0.97/0.82/.53 bar CO₂, 0.04, 0.03, and 0.02 mbar H₂S, 1 wt. % NaCl, 300rpm stir bar, 7days.)

Surface profilometry in Figure 14 shows that localized corrosion was observed at 30 °C while the corrosion found at 60 °C and 80 °C was extensive but uniform.

Figure 15 shows SEM cross-section images of specimens at different temperatures. At 60 °C, the surface morphology seems to indicate that pits initially form, similarly to what was observed at 30 °C, grew larger and agglomerated to form a uniformly rough surface. At 80 °C, the morphology of the corrosion attack appeared different although the corrosion rate was similar to that observed at 60 °C.

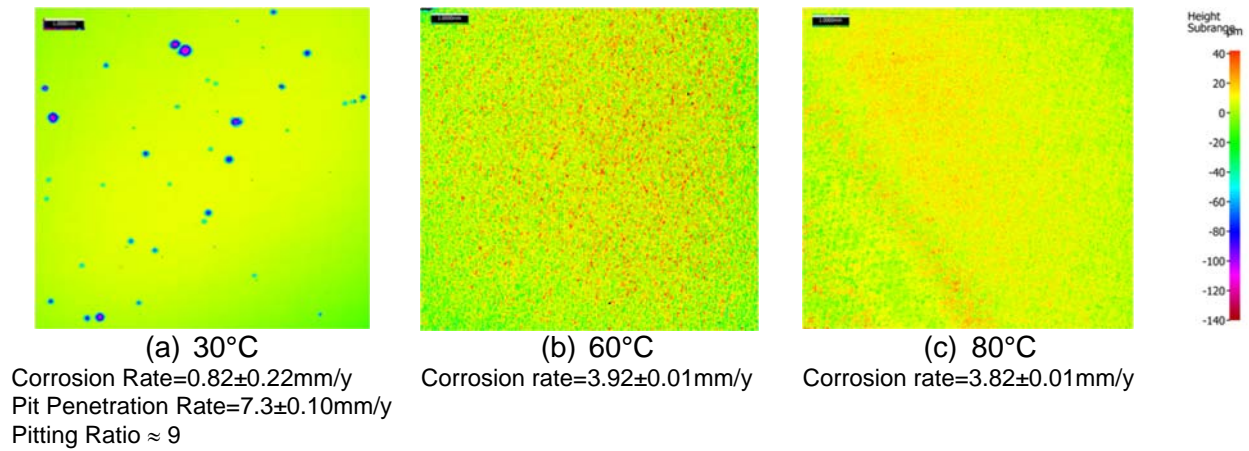


Figure 14. Surface profilometry scanning images of different temperatures after 7 days exposure after corrosion product layer removed. (pH=5, X-65 carbon steel, 30/60/80°C, 0.97/0.82/.53 bar CO₂, 0.04 mbar (40ppm) H₂S, 1 wt.% NaCl, 300rpm stir bar.)

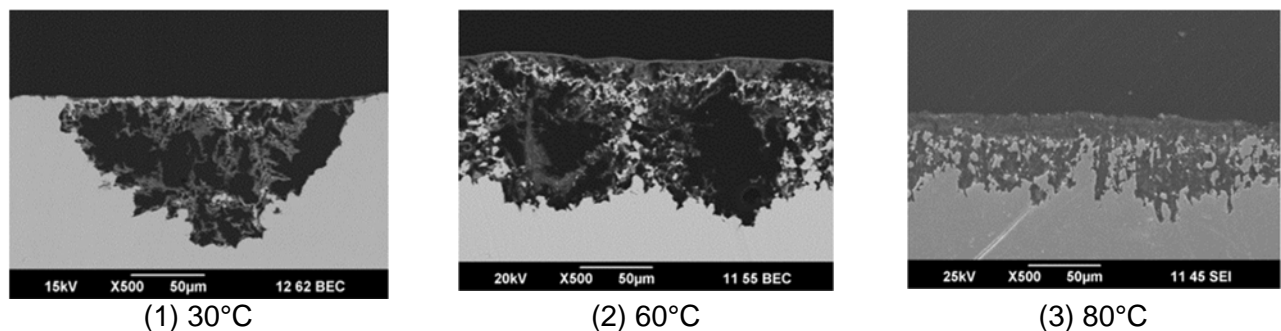


Figure 15. SEM cross-section images of specimens at different temperatures after 7 days exposure. (X65 carbon steel, 30/60/80°C, 0.97/0.82/.53 bar CO₂, pH5, 1 wt.% NaCl, 300rpm stir bar.)

Effect of Salt Concentration on Localized Corrosion

The effect of sodium chloride concentration on localized corrosion was investigated at pH 5, 0.04 mbar (40 ppm) H₂S and 0.97 bar of CO₂ by performing tests at 0, 1 and 10wt% NaCl. The saturation degrees of mackinawite and iron carbonate are illustrated in Figure 16. Here, the saturation degree does not change with NaCl concentration because neither the ionization equilibrium constant equation²⁵ nor the solubility constant equation²⁶ of mackinawite are dependent on the ionic strength (according to the currently available expressions). According to Figure 16, iron carbonate is saturated in the bulk at 0 wt. % NaCl, iron carbonate is almost saturated in bulk solution for 1 wt. % NaCl, and none of the corrosion products are saturated in 10 wt. % NaCl experiments. However, from Figure 17, it seems that initiation of localized corrosion was independent of the concentration of NaCl present in the system.

Surface profilometry scanning images of specimens at different salt concentrations are shown in Figure 17. As the concentration of salt increased, pit density increased without much change in pit penetration rates. This indicated that pitting density was related to conductivity of the solution and galvanic coupling between the steel and iron sulfide layer^{27,28}. The decrease in general corrosion rate with an increase in NaCl concentration was expected according to Fang.^{24,29}

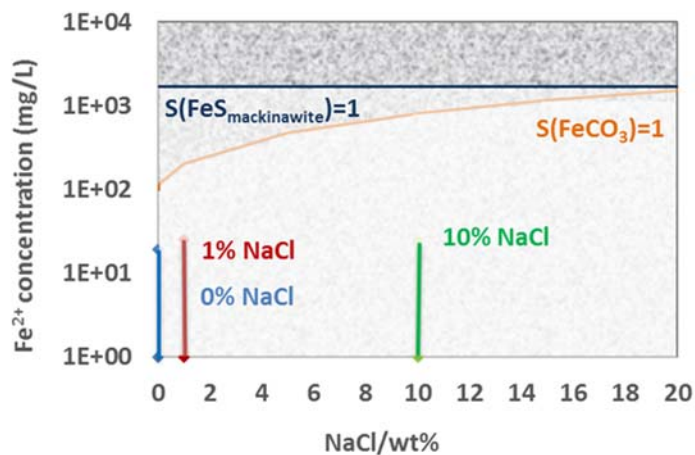


Figure 16. Saturation degree of both mackinawite (blue line and above) and iron carbonate (orange line and above) in bulk solution. (X65 carbon steel, 30°C, pH5, 0.97 bar CO₂, 0.04 mbar H₂S, 0/1/10 wt. % NaCl, 300rpm stir bar, 7days)

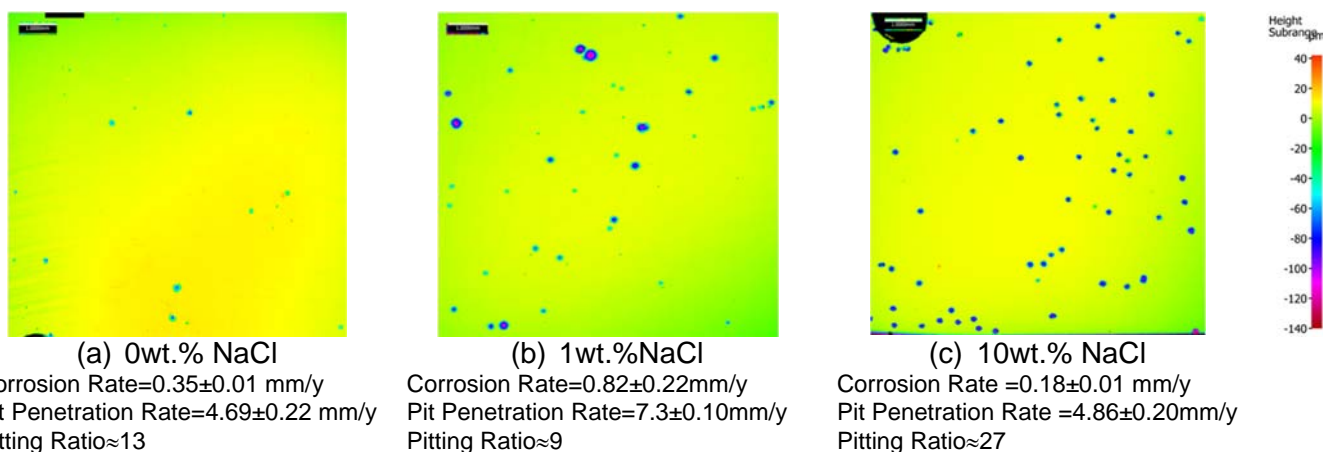


Figure 17. Surface profilometry scanning images of specimens at different salt concentrations after 7 days exposure after corrosion product layer removed. (X65 carbon steel, 30°C, pH5, 0.97 bar CO₂, 0.04 mbar H₂S, 0/1/10 wt.% NaCl, 300rpm stir bar, 7days.)

SEM cross-section images of specimens at different salt concentrations are shown in Figure 18. There does not seem to be a major difference in the pit morphology as related to the salt concentration.

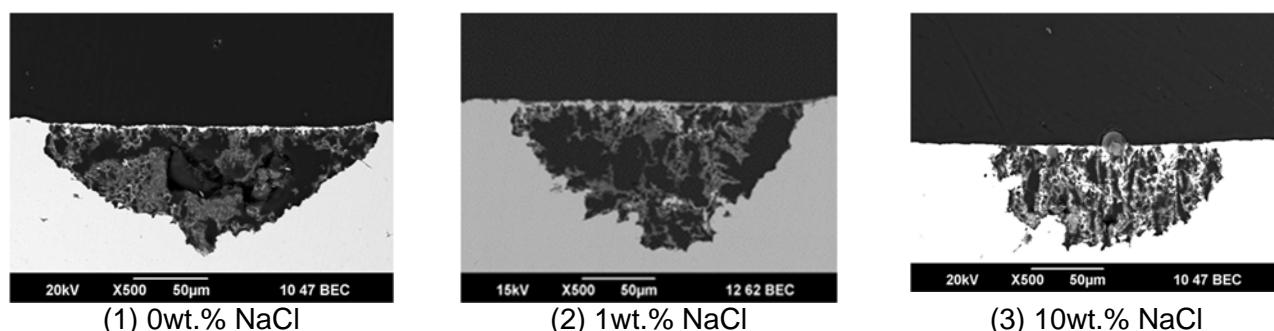


Figure 18. SEM cross-section images of specimens at different salt concentrations after 7 days exposure. (X65 carbon steel, 30°C, pH5, 0.97 bar CO₂, 0.04 mbar H₂S, 0/1/10 wt.% NaCl, 300rpm, 7days.)

Effect of Microstructure on Localized Corrosion

To identify the effect of material microstructure and composition on localized corrosion, experimental results were compared with pure iron and X-65 steel at 0.04 mbar (40 ppm) H₂S, 0.97 bar of CO₂, 30°C, pH5 and 1 wt.% NaCl. The tests were done with pure iron as control since its microstructure does not contain Fe₃C, which is present in the ferritic with iron carbide precipitates microstructure of X65. X65 and pure iron specimens were tested in independent experiments. The bulk FeS and FeCO₃ saturation degrees were always below unity.

Surface profilometry images of X65 and pure iron specimens are shown in Figure 19. No pits were found on the pure iron specimen although the experimental conditions were exactly the same as X65, where severe localized corrosion occurred. The reasons for this are revealed through the analysis of the corrosion product layer in Figure 20.

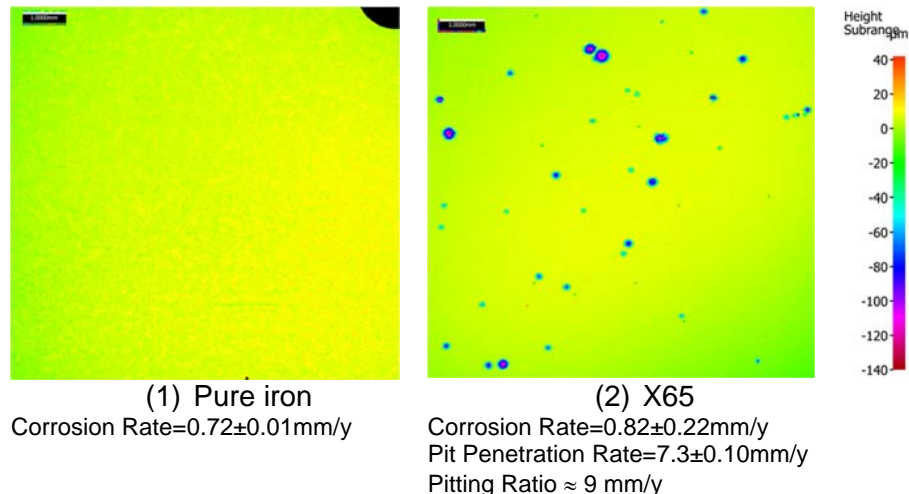


Figure 19. Surface profilometry scanning images of specimens of X65 and pure iron specimens after 7 days exposure after corrosion product layer removed. (Pure iron/X-65 carbon steel, 30°C, pH5, 0.97 bar CO₂, 0.04mbar H₂S, 1 wt.% NaCl, 300rpm.)

The cross-section images by SEM backscattering and EDS mapping for the sulfur element of X65 and pure iron are displayed in Figure 20. As shown in Figure 20 (1) and (3), no corrosion product layer was observed on the surface of the pure iron specimen. As for X65, there was a thin layer observed on the surface of the specimen. This thin layer is hypothesized to constitute of FeS imbedded inside a Fe₃C network (Figure 21). The resolution of the EDS image was not sufficiently high to be certain and this will be further studied by transmission electron microscope (TEM), X-ray photoelectron spectroscopy (XPS) and Raman spectroscopy in the future.

According to EDAX analysis result in Figure 21, the corrosion product layer contained as major elements: iron, sulfur and carbon, lesser amounts of oxygen, and trace amounts of other alloying elements. This indicates the possible existence of Fe₃C, FeS, FeCO₃, and/or Fe_xO_y. Further study of the layer should be done to reveal the detailed structure of this protective layer, so that the mechanism for localized corrosion of mild steel in marginally sour environments can be better understood.

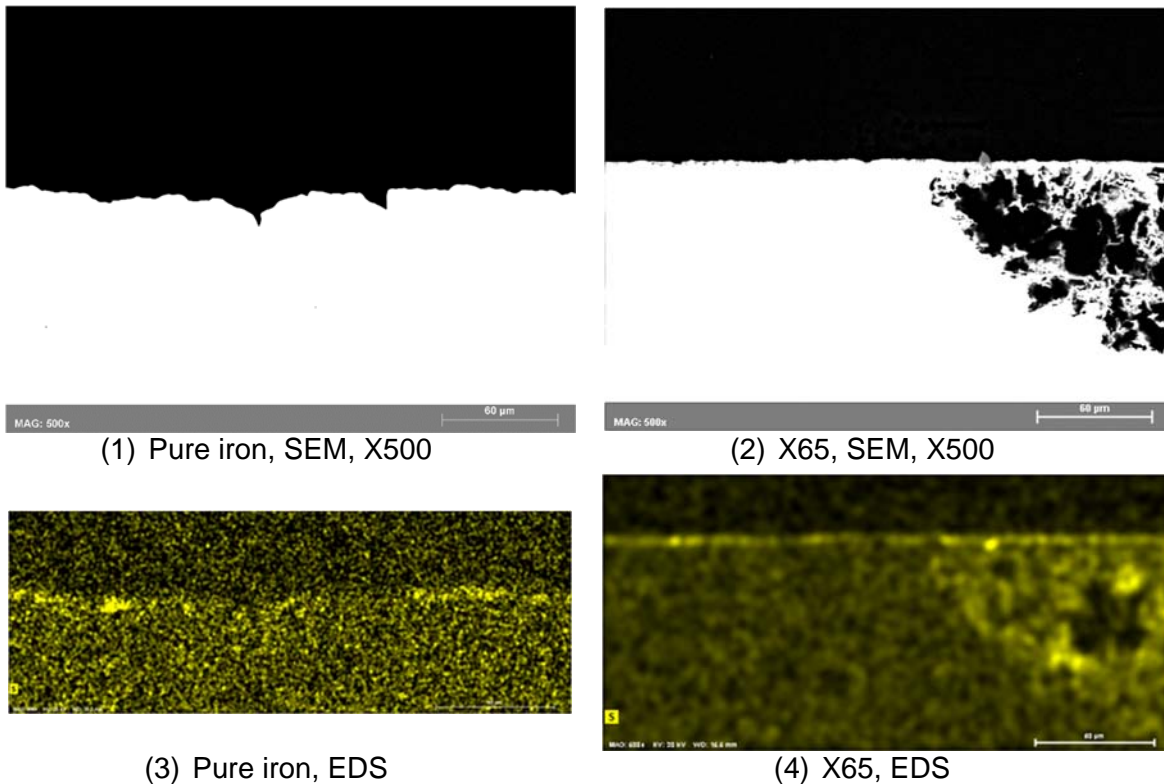
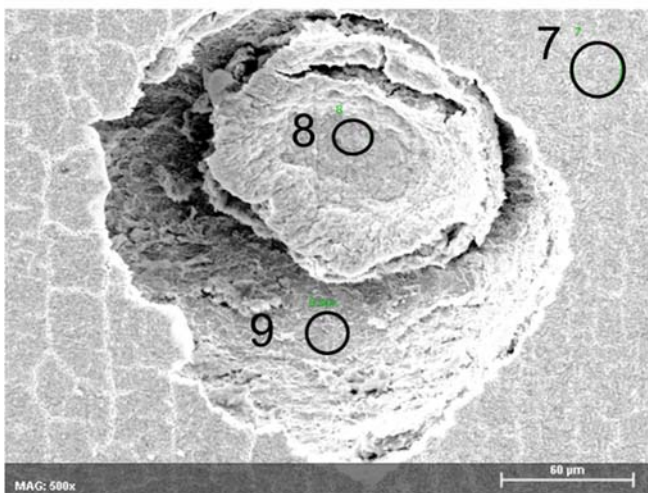


Figure 20. The cross-section images by SEM backscattering and EDS mapping for the sulfur element. (Pure iron/X-65 carbon steel, 30°C, pH5, 0.97 bar CO₂, 0.04mbar H₂S, 1 wt.% NaCl, 300rpm stir bar, 7 days.)



| Sampling Spots | 7 | 8 | 9 |
|----------------|----------|----------|----------|
| Element | Atom [%] | Atom [%] | Atom [%] |
| Carbon | 14.45 | 19.77 | 0.00 |
| Oxygen | 5.41 | 15.40 | 0.00 |
| Aluminum | 0.03 | 0.00 | 0.12 |
| Sulfur | 16.49 | 0.00 | 24.55 |
| Chromium | 0.03 | 1.61 | 0.00 |
| Manganese | 0.75 | 0.54 | 3.86 |
| Iron | 61.99 | 62.39 | 71.48 |
| Molybdenum | 0.85 | 0.29 | 0.00 |
| Sum | 100.00 | 100.00 | 100.00 |

Figure 21. EDAX analysis results of corrosion product layer inside and surrounding the pit on X-65 carbon steel specimens after 10 days corrosion test. (30°C, pH5, 0.97 bar CO₂, 0.04mbar H₂S, 1 wt.% NaCl, 300rpm stir bar.)

CONCLUSIONS

A parametric study of localized corrosion of mild steel in marginally sour environments was completed. Fundamental characteristics of localized corrosion were revealed, especially related to protective layer formation. It was found that a very thin layer of FeS, expected to be mackinawite, precipitated within the porous iron carbide network of mild steel to retard general corrosion of the steel surface. This

precipitation occurred because a higher saturation of iron sulfide within the porous iron carbide structure. This finding confirms the need for a more precise surface saturation calculation rather than the use of existing bulk water chemistry models for saturation.

The experimental results helped to clarify the effect of some operating parameters related to the occurrence of localized corrosion in marginally sour environments. Localized corrosion was observed at the following conditions:

- At H₂S partial pressure of 0.02 to 0.09 mbar (but not at 0 mbar and 0.15 mbar);
- At CO₂ partial pressure of 0.53 to 0.97 bar (but not at 0 bar i.e. in pure H₂S solution);
- At pH 4 and 5 (but not at pH6);
- At 30°C only (but not 60 or 80°C);
- At NaCl concentrations from 0 to 10%;
- On specimens containing a Fe₃C phase (but not on pure iron).

The partial pressure of H₂S and CO₂, pH, temperature, and ionic strength all can affect saturation degree of the FeS in solution. Localized corrosion only initiated when H₂S was present in this system and propagated only when CO₂ was present. These were proven by the fact that no localized corrosion was found in CO₂ only experiments and only initiation of corrosion was found in the H₂S only experiments.

Chloride concentration was not found to be related to pit initiation. This was proven by the fact that localized corrosion was found in experiments at 0 wt.% of NaCl.

This leads to the conclusion that an interaction between the FeS layer (most likely mackinawite) and the Fe₃C network is suspected to play a role in the initiation of localized corrosion. Propagation then followed due to galvanic coupling between the underlying steel and the conductive iron sulfide layer. A more detailed pit initiation mechanism needs to be revealed in further study.

ACKNOWLEDGEMENTS

The author would like to thank the following companies for their financial support:

Anadarko, Baker Hughes, BP, Chevron, CNOOC, ConocoPhillips, DNV GL, ExxonMobil, M-I SWACO (Schlumberger), Multi-Chem (Halliburton), Occidental Oil Company, Petrobras, PTT, Saudi Aramco, Shell Global Solutions, SINOPEC (China Petroleum), TransCanada, TOTAL, and Wood Group Kenny.

REFERENCES

1. S. N. Smith, and M. W. Joosten, "Corrosion of Carbon Steel by H₂S in CO₂ Containing Oilfield Environments - 10 Year Update", in the NACE International Annual Conference and Exposition, p. 5484, Houston: NACE International, 2015.
2. N. N. Bich, and K. Goerz, "Caroline Pipeline Failure: Findings on Corrosion Mechanisms in Wet Sour Gas Systems Containing Significant CO₂", in the NACE International Annual Conference and Exposition, p. 96026, Houston: NACE International, 1996.
3. B. Brown, D. Young, and S. Nešić, "Localized Corrosion in an H₂S / CO₂ Environment", in the 17th international corrosion congress, NACE International, Houston, TX, 2009.
4. N. Yaakob, F. Farelas, M. Singer, S. Nesic, D Young, "Localized Top of the Line Corrosion in Marginally Sour Environments", in the NACE International Annual Conference and Exposition, p. 96026, Houston: NACE International, 2016.

5. S. Navabzadeh Esmaeely, W. Zhang, B. Brown, M. Singer, and S. Nešić, "Localized Corrosion of Mild Steel in Marginally Sour Environments," *CORROSION*, September 2017, Vol. 73, No. 9, pp. 1098-1106.
6. S. Navabzadeh Esmaeely, W. Zhang, B. Brown, M. Singer, and S. Nešić, "Localized Corrosion of Mild Steel in Marginally Sour Environments," in the NACE International Annual Conference and Exposition, paper number to be decided, Houston: NACE International, 2018.
7. W. Yan, B. Brown, S. Nestic, "Investigation of the Threshold Level of H₂S for Pitting of Mild Steel in CO₂ Aqueous Solutions", in the NACE International Annual Conference and Exposition, p.11472, Houston: NACE International, 2018.
8. J. R. Galvele, "Transport Processes and the Mechanism of Pitting of Metals", *J. Electrochem. Soc.*, vol. 123 (4), p. 464–474, 1976.
9. D. D. Macdonald, "The Point Defect Model for the passive state", *Journal of The Electrochemical Society*, 139 (12), 3434. 1992. <https://doi.org/10.1149/1.2069096>.
10. H. H. Strehblow, "Passivity of Metals", in *Advances in Electrochemical Science and Engineering*, Volume 8. Edited by Richard C. Alkire, Copyright (2002 Wiley-VCH Verlag GmbH & Co. KGaA, ISBNs: 3-527-30211-5 (Hardback); 3-527-60078-7 (Electronic).
11. J. Ning, Y. Zheng, D. Young, B. Brown, and S. Nešić, "Thermodynamic Study of Hydrogen Sulfide Corrosion of Mild Steel", *CORROSION*, April 2014, Vol. 70, No. 4, pp. 375-389.
12. J. Han, S. Nestic, Y. Yang, B. Brown, "Spontaneous passivation observations during scale formation on mild steel in CO₂ brines", *Electrochimica Acta* 56 (2011) 5396–5404.
13. A. Dugstad, "Mechanism of protective film formation during CO₂ corrosion of carbon steel", *Corrosion/98*, Paper no. 31, NACE International, Houston, Texas, 1998.
14. Y. Sun, "Localized CO₂ corrosion in horizontal wet gas flow", Ph.D. dissertation, Dept. Chem. & Biomol. Chem. Eng., Ohio Univ., Athens, OH, 2003.
15. W. Sun and S. Nestic, "A mechanistic model of uniform hydrogen sulfide/carbon dioxide corrosion of mild steel," *Corrosion*, vol. 65, no. 5, pp. 291–307, 2009.
16. P. Marcus and E. Protopopoff, "Potential-pH diagrams for adsorbed species: application to sulfur adsorbed on iron in water at 25 °C and 300 °C," *J. Electrochem. Soc.*, vol. 137, no. 9, pp. 2709–2712, 1990.
17. D. E. Jiang and E. A. Carter, "Adsorption, diffusion, and dissociation of H₂S on Fe (100) from first principles," *J. Phys. Chem. B*, vol. 108, no. 50, pp. 19140–19145, 2004.
18. Y. Zheng, J. Ning, B. Brown, and S. Nešić, "Advancement in predictive modeling of mild steel corrosion in CO₂- and H₂S-containing environments", *CORROSION*, May 2016, Vol. 72, No. 5 (May 2016) pp. 679-691.
19. Z. Ma, Y. Yang, B. Brown, S. Nestic, and M. Singer, "Investigation of FeCO₃ and FeS Precipitation Kinetics by EQCM", in the NACE International Annual Conference and Exposition, paper number to be decided, Houston: NACE International, 2018.
20. X. Zhong, "How to maintain a stable solution chemistry when simulating CO₂ corrosion in a small volume laboratory system", in *NACE Corrosion Conf.*, Vancouver, BC, Canada, Paper no. 7780, Mar., 2016.
21. API Specification 5L: Specification for Line Pipe, Forty-Third Edition, March 2004 Effective Date: October 2004 Errata December, 2004.
22. A. A. Al-Asadi, "Iron Carbide Development and its Effect on Inhibitor Performance", Master's Thesis, Dept. Chem. & Biomol. Chem. Eng., Ohio Univ., Athens, OH, December 2014.
23. Standard Guide for Examination and Evaluation of Pitting Corrosion. ASTM G46, 2013.
24. H. Fang, B. Brown and S. Nešić, "Effects of Sodium Chloride Concentration on Mild Steel Corrosion in Slightly Sour Environments", *CORROSION*, Jan 2011, Vol. 67, No. 1 (January 2011) pp. 015001-1-015001-12.
25. Y. K. Kharaka, W. D. Gunter, P. K. Aggarwal, E. H. Perkins, and J. D. DeBaal, "Solmineq 88: A computer program for geochemical modeling of water rock interactions", Menlo Park, CA: Alberta Research Council, 1989.

-
26. L. G. Benning, R. T. Wilkin, and H.L. Barnes, "Reaction pathways in the FeS system below 100 °C," *Chem. Geol.*, vol. 167, no. 1–2, pp. 25–51, 2000.
 27. J. Ning, Y. Zheng, D. Young, B. Brown, and S. Netic, "The Role of Iron Sulfide Polymorphism in Localized H₂S Corrosion of Mild Steel", *CORROSION*, February 2017, Vol. 73, No. 2, pp. 155-168.
 28. S. Navabzadeh Esmaeely, G. Bota, B. Brown, S. Netic, "Effect of Pyrrhotite on Mild Steel Corrosion in Aqueous CO₂ and H₂S Solutions", in the NACE International Annual Conference and Exposition, paper number to be decided, Houston: NACE International, 2018.
 29. H. Fang, B. Brown and S. Nešić, "Sodium Chloride Concentration Effects on General CO₂ Corrosion Mechanisms", *CORROSION*, Mar 2013, Vol. 69, No. 3 (March 2013) pp. 297-302.
 22. B. Brown, "The Likelihood of Localized Corrosion in an H₂S/CO₂ Environment", in the NACE International Annual Conference and Exposition, p. 5855, Houston: NACE International, 2015.